

Spatio-temporal Consistency to Detect Potential *Aedes aegypti* Breeding Grounds in Aerial Video Sequences

Wesley L. Passos¹, Eduardo A. B. da Silva¹, Sergio L. Netto¹, Gabriel M. Araujo², Amaro A. de Lima².

Abstract—Every year, the *Aedes aegypti* mosquito infects thousands of people with diseases such as dengue, zika, chikungunya, and urban yellow fever. The main form to combat these diseases is to avoid the transmitter reproduction by searching and eliminating the potential mosquito breeding grounds. In this work, we introduce a comprehensive database of aerial videos recorded with a drone, where all objects of interest are identified by their respective bounding boxes, and describe an object detection system based on deep neural networks. We track the objects by employing phase correlation to obtain the spatial alignment between them along the video frames. By doing so, we are capable of registering the detected objects, minimizing false positives and correcting most false negatives. Using the ResNet-101-FPN as a backbone, it is possible to obtain 0.78 in terms of *F1-score* on the proposed dataset.

Index Terms—*Aedes aegypti*, image and video processing, computer vision, object detection and tracking.

I. INTRODUCTION

The mosquito *Aedes aegypti* is the major transmitter of diseases caused by the arbovirus (an acronym for the arthropod-borne virus), such as dengue, zika, chikungunya, and yellow fever [1]. An estimate says that about 390 million people are infected per year in the world [2]. In 2019, the Americas alone reported more than 2.7 million cases of dengue; more than 2 million only in Brazil [3]. Zika virus infection during pregnancy correlates to microcephaly (smaller than average head size) and other congenital malformation in the infants; children in these conditions rarely develop normally [4]. Chikungunya may trigger neurological and heart problems. It may also incapacitate those infected for long periods and may lead older people to death [5]. Yellow fever caused 483 deaths in Brazil between July 2017 and June 2018, which is a significant increase when compared to 262 deaths in the same period of 2016/2017 [6]. Yet, these diseases have a great impact on economics. A survey conducted in 17 countries in the Latin and Central Americas estimates that the cost of dengue epidemics in these countries exceeds US\$ 3 billion annually, US\$ 1.4 billion only in Brazil [2]. These facts make arboviruses transmitted by the *Aedes aegypti* one of the leading global health problems.

Except for the case of yellow fever, there is no vaccine nor specific antiviral drugs for the diseases above. Thus, the current best form to combat them is through the control and

elimination of possible mosquito foci, which acts directly in the prevention of all these diseases [7]. The *Aedes aegypti* reproduces in clean and stagnant water, thus any containers that allow the storage of water (water tanks, buckets, ornamental fountains, plant dishes, water canisters for animals, tires, and others) are potential breeding grounds. Such objects are everywhere, which can make monitoring and controlling the mosquito, in the absence of proper technical support, expensive, time-consuming, and inefficient. Allying the knowledge of an expert with a tool that accelerates the search for potential mosquito foci can be very valuable in the current scenario.

In this work, we propose the use of images and videos captured by an unmanned aerial vehicle (UAV), also known as *drone*, with several sensors and a camera. Currently, *drones* have been used by organizations to inspect hard-to-reach sites. However, the acquired material is usually examined by an expert who identifies the reproduction points by visual inspection, which tends to be time-consuming, tiring, and, consequently, prone to failure. In this sense, this work proposes a system to automate the analysis process by applying machine learning and computer vision techniques to help the specialist in the localization of relevant mosquitoes foci. For this, we present a video database (including real scenarios), with objects and a greater variation in altitude of the *drone*. To illustrate the concept, tires are used as an object of interest. Tire detection is done using the *Faster R-CNN* architecture in all frames of the video. Due to the characteristics of the database used, we can assume that the movement between frames is purely translational. The *phase correlation* technique is used to measure this displacement and perform spatial compensation between frames in a time window. This compensation allows adopting a heuristic to register between detections, eliminating a good part of false positives and correcting the vast majority of false negatives.

The paper is organized as follows: Section II contains a literature review, describing some related work in the area. Section III describes the database. The proposed method is described in Section IV. The V section contains results obtained and a discussion about those results. The conclusion is in Section VI.

II. RELATED WORK

In this section, we briefly talk about the literature related to this work. First, we talk about the metrics in object detection and tracking. Next, we point out the works related to the detection of mosquito breeding grounds.

¹PEE/COPPE/DEL/POLI, Universidade Federal do Rio de Janeiro, Cx. P. 68504, Rio de Janeiro, RJ, 21945-970, Brasil. ²Centro Federal de Educação Tecnológica, Nova Iguaçu, RJ, 26041-271, Brasil. E-mails: {wesley.passos, sergioln, eduardo}@smt.ufrr.br. {gabriel.araujo, amaro.lima}@cefet-rj.br.

A. Object detection and tracking metrics

The average precision (AP) is used as a metric in many works that performs object detection in video sequences. Generally, each frame is treated separately. Such an approach ignores the temporal characteristics. The delay is defined as the number of frames from when an object appears to when it is detected. The authors in [8] claim that most detection drastically increases detection delay but preserve AP well, so AP is not sensitive enough to reflect temporal characteristics. This is important for many latency-critical applications, such as autonomous vehicle perception. Hence, exploiting temporal information is an important direction to improve accuracy-cost trade-off. The work in [8] proposed a delay metric for object video object detection, the Average Delay (AD). The authors in [8] assume that the delay is a discrete exponential distribution over the probability of detection of every object in every frame. The AD is obtained by averaging the delay over a 30-frames window with a specific false positive (FP) ratio.

The work in [9] proposed 2 performance metrics for multiple object tracking. Multiple Object Tracking Precision (MOTP), which can be defined as the average distance between all detected objects and is correspondent ground truth over the number of matches in a time window. On the other hand, the Multiple Object Tracking Accuracy (MOTA) can be obtained by averaging the false positives, false negatives, and the number of mismatch errors (when the tracker swap the identities of two objects or when the tracker reinitialize a lost object with a new identity) over the number of objects present in a time window.

The MOTP and MOTA also were taken into account in [10]. However, the authors considered a threshold over the Intersection over Union (IoU) rather than the distance between detection and the ground truth to determine whether the detection is correct or not.

The method in [11] takes into account spatial and temporal overlaps in the metrics. These overlaps are computed through IoU between the detection and the ground truth in a frame and over a time window. An object is considered as correctly tracked if the overlaps are larger than thresholds. They are referred to as correct detected track (CDT) or true positive (TP). A track is considered as false alarm track (FAT) or false positive (FP) if the spatial or temporal overlaps are smaller than given thresholds. Track detection failure (TDF) occurs when both overlap tests fail. Other metrics such as track fragmentation (TF), ID change (IDC), latency of the system track (LT), closeness of track (CT), track matching error (TME), and track completeness (TC) were also defined.

Since the application of our work is not latency-critical, such as the one in [8], there is no need to consider AD. We also used a threshold over the IoU to determine whether the detections are correct or not. However, instead of using two types of overlaps (a spacial and a temporal one), we defined the IoU between tracks. Besides, we spatially align the frames using Phase Correlation before computing IoU.

B. Mosquito breeding grounds detection

Regarding mosquito breeding grounds detection, we start pointing out the work in [12], where the authors propose

a system to identify potential mosquitoes breeding sites in geotagged images received from the population. The images are converted into feature vectors using the bag of visual words model through the scale-invariant feature transform (SIFT) descriptor to train a support vector machine (SVM) classifier. According to classification, the system outputs a heat map highlighting the regions with the highest risk of having mosquitoes habitats. The authors of [13] use a trained SVM classifier to detect water puddles in images obtained from videos that can have stagnant water, acquired by a quadcopter. The work in [14] trains an ensemble of naive Bayes classifiers with speeded-up robust features (SURF) features extracted from thermal and gray level images to detect stagnant water. The authors of [15] use images from Google Street View, Google image search, and Common Objects in Context (COCO) dataset to train and test the Faster R-CNN to detect tires, buckets, potted plants, garbage bins, vases, bowls, and cups. The detected objects are used to compose a dashboard showing the risk areas. In a test set, the system described in [15] obtained an accuracy of up to 0.91 in terms of *F-score*. Despite having promising results, due to the dataset characteristics, the method is only applicable in public ways.

Aerial images have the potential to reveal big mosquito breeding grounds in abandoned private areas and/or difficult to access areas. The papers in [16], [17] proposed more adequate datasets for this type of application. One can find a method using histograms of HSV channels and optical flow as feature extractors and Random Forest to classify tires and stagnant water. The results are promising, but the dataset is small and still have little variability. The dataset in [16] have greater variability, but the dataset size is still an issue when using deep learning to detect the objects of interest. The work in [18] proposed a data augmentation technique to solve this problem. Despite the little variability of the objects of interest in the dataset proposed by [16], the work in [19] proposed a detector based on Faster R-CNN to detect tires with promising results.

In this work, we present an extension of the dataset proposed by [16] (in interrupt development since 2018). In the current version, the dataset has more videos and many more objects of interest. The videos were taken in different locations altitude and objects arrangements. The videos are densely annotated (frame by frame), which is greatly valuable to develop and evaluate an automatic object detector. We also employed a *Faster R-CNN* based detector. However, another important contribution of this work is in the tracking method employed to mitigate the detection inconsistencies. The Phase Correlation is applied in successive frames to spatially align them in a time window. It is followed by a heuristic to i) associate different detections of the same object; ii) get rid of false detections (False Positives) and; iii) correct missing detections (False Negatives).

III. VIDEO DATABASE

In this section, we present our video database devised for detecting mosquito breeding grounds in aerial videos. This database contains a representative video data set, acquired using a *drone*, with extensive types of objects considered as potential *Aedes aegypti* breeding grounds, including their

bounding boxes annotations. Also, we have the drone telemetry, which allows the localization of these objects.

Since drones have many flight restrictions, the main difficulty in constructing such a database is to obtain access to extensive types of real scenarios. Even if drone access is available to several locations, it is also necessary to know where the disease-related objects are. In this way, the solution adopted to this database is to capture some videos in simulated scenes, where some objects were manually inserted in locations where foot access is available.

The drone camera was calibrated using Zhang's method [20] to minimize most lens distortions. To allow a supervised approach, the objects of interest in the recorded videos are densely (frame-by-frame) annotated with bounding boxes. Each video in the database has an annotation file, containing the ground truth bounding box of the objects of interest for each frame, and a telemetry file, that stores the values of several drone parameters during the recording.

In this way, a proper database for the problem of supervised learning to detect and classify objects in aerial videos should have: (i) control of the maximum numbers of parameter or at least have their measurement; (ii) an expressive number of samples and representativeness of each object class; (iii) variability of the background, objects, luminosity, and height; (iv) no camera distortions; and (v) reliable annotation.

So far, our database is composed of 22 video sequences acquired by a drone platform DJI Phantom 4 Pro recorded in 10 different locations. Three of these locations are real and in the others, the objects of interest were manually inserted into the scene in random positions before recording the videos. The database contains videos recorded with resolution 3840×2160 at 50 Hz and 4096×2160 at 30 Hz. The altitudes of the *drone* also varied, with 4 videos being obtained at an altitude of 10 m, 3 with 15 m, 1 with 16 m, 4 with 20 m, and 10 with an altitude of 40 m. It contains 131,478 frames with a total of 87,151 bounding boxes annotated of several objects manually annotated such as bottles, buckets, pools, puddles, tires, and water tanks. Table I shows the type of objects and their quantity in the database. Figure 1 shows examples of video sequences frames in this database and Figure 2 shows a few objects that are potential mosquito breeding grounds. Table I show the number of objects in the database.

Table I: Number of annotated objects in the database.

	Bottle	Bucket	Pool	Tire	Water tank
Annotated	9,295	11,409	6,412	21,941	38,094
Unique	81	100	56	224	400

IV. PROPOSED METHOD

In this section, we present the steps for detecting possible breeding grounds of the *Aedes aegypti*. We talk briefly about the object detector used to detect such possible mosquito breeding sites and show the technique for tracking the objects.

A. Object detector

Object detection consists of both locating and classifying one or more instances of objects in images or videos. The

detector assigns a set of bounding boxes to each image, containing their coordinates and labels.

Convolutional neural networks (CNN) have demonstrated good performance in object detection [21]. The *Faster region-based convolution neural network (Faster R-CNN)* [22] is a CNN-based meta-architecture that has been showing excellent results in various applications and competitions [21]. The *Faster R-CNN*, illustrated in Figure 3, is basically composed of a feature extractor, a region proposal generator (*region proposal network*, RPN), and a classification and regression module (cls/reg). The feature extractor, which is usually a deep CNN, extracts convolutional feature maps from the input images. Based on these maps, the RPN generates potential regions of interest (RoI), which are delivered to the classification and regression module (densely connected layers) that identify the classes of the RoIs and refine them, predicting a shift.

B. Object tracking

Due to the characteristics of the database, it is possible to assume that the movement between adjacent frames is purely translational. Techniques such as *phase correlation* [23] allow us to register, in a computationally efficient way, the translation between two images, without rotations or scale changes, as is the case with the videos in our database.

The translational displacement of the detected objects between successive frames can be obtained as follows. Considering that a frame $\mathbf{f}_{n+1}(x, y)$ is a translated version of the frame $\mathbf{f}_n(x, y)$ frame, with displacement $\mathbf{d} = (x_0, y_0)$,

$$\mathbf{f}_{n+1}(x, y) = \mathbf{f}_n(x - x_0, y - y_0). \quad (1)$$

According to the translation property of the Fourier transform, the transforms of \mathbf{f}_n e \mathbf{f}_{n-1} are related as

$$\mathbf{F}_{n+1}(\xi, \eta) = e^{-j2\pi(\xi x_0 + \eta y_0)} \mathbf{F}_n(\xi, \eta). \quad (2)$$

Therefore, the normalized cross-power spectrum between the two images is given by

$$\frac{\mathbf{F}_{n+1}(\xi, \eta) \mathbf{F}_n^*(\xi, \eta)}{|\mathbf{F}_{n+1}(\xi, \eta) \mathbf{F}_n(\xi, \eta)|} = e^{-j2\pi(\xi x_0 + \eta y_0)}, \quad (3)$$

where \mathbf{F}^* is the complex conjugate of \mathbf{F} . In theory, the inverse Fourier transform of Equation (3) is the Kronecker delta $\delta(x_0, y_0)$. In practice, this inverse transform tends to have all its elements approximately zero, except in the position that corresponds to displacement.

In this work, we apply the phase correlation technique to obtain spatial displacement between frames. The computed displacement is employed to spatially align the detection over their frames. We consider that detections in these frames belong to the same object when $\max(IoU) \geq 0,5$ regarding the bounding boxes. In doing so, one can observe the behavior of the detections over the frames and employ some heuristic to mitigate the inconsistencies (false positives and false negatives). To illustrate the procedure, let us consider the example in Figure 4. The horizontal solid black lines represent the frames of a video. The small solid red lines are the model outputs in each frame (detections). If, after employing the



Figure 1: Screenshots examples of video sequences in the database.



Figure 2: Examples of potential mosquito breeding grounds in the database.

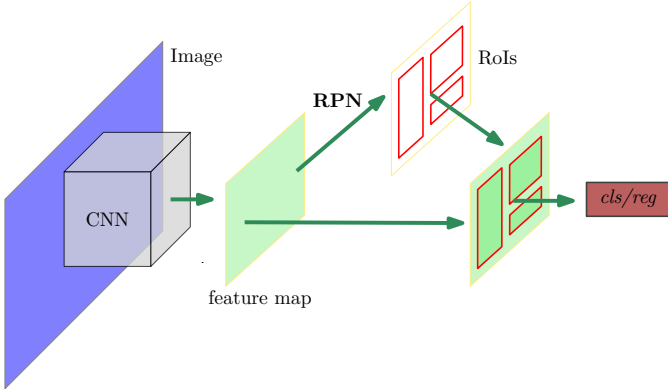


Figure 3: *Faster R-CNN*.

phase correlation, the $\max(IoU) \geq 0.5$ between detections in consecutive frames, then these detections indicate to be of the same object (object identification- ID). If there is not a detection that holds this condition, we have a possibly missed detection. An estimate, represented by a dashed red line, is generated by projecting a previous detection (or estimate). Each collection of detections and/or estimates is a track (pink paths in Figure 4).

Let m_i the number of frames of a track i (including detections and estimates) and l_i the number of detections

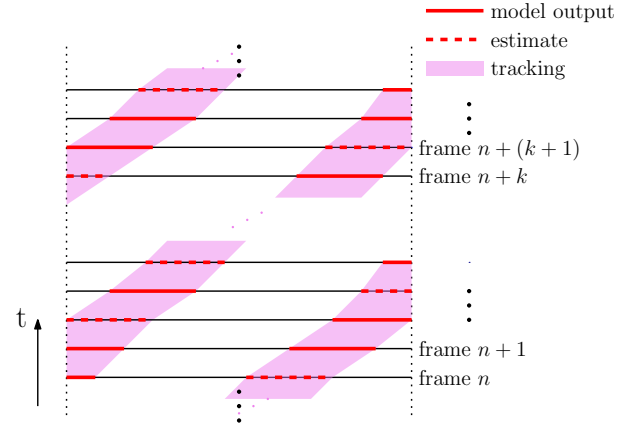


Figure 4: Black solid lines are frames. Solid red lines are detections (model output) over these frames. The red dashed lines are estimates generated by projecting a detection or another estimate from a previous frame. The collection of detections and/or estimates having the same object ID is a track (pink path).

output by the model inside the track i . The track i is considered as belonging to a real object of interest if $v = (l_i/m_i)$ is equal or greater than a threshold t_v . It is discarded otherwise.

The object track (pink) and ground truth track (green) are

shown in Figure 5.

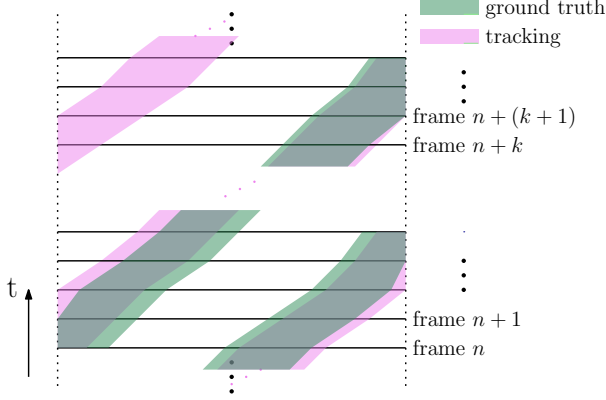


Figure 5: The object tracks are pink and ground truth tracks are green. If the upper left object track has $v < t_v$, then it is discarded. Since there is not a corresponding ground truth track, it is a false positive if has $v \geq t_v$.

V. RESULTS AND DISCUSSION

One metric widely used in the context of object detection is the *average precision* with $\text{IoU} \geq 0.5$ (AP_{50}) [19]. However, this metric by itself does not provide the idea of the number of true positives (TP), false positives (FP), and false negatives (FN), which will also be analyzed. Note that true negatives (TN) are not applied in this context. To aggregate the TP, FP and FN information, we report the values of *precision* (Pr), *recall* (Rc) and *F1-score* (F_1) given, respectively, by:

$$\text{Pr} = \frac{\text{TP}}{\text{TP} + \text{FP}}, \quad \text{Rc} = \frac{\text{TP}}{\text{TP} + \text{FN}} \quad \text{and} \quad (4)$$

$$F_1 = 2 \cdot \frac{\text{Pr} \cdot \text{Rc}}{\text{Pr} + \text{Rc}}. \quad (5)$$

A. Object detection with the Faster R-CNN

In total, we trained 4 different Faster R-CNN models, using ResNets, with 50 or 101 layers, as a feature extractor (*backbone*). We feed the RPN, and the regression and classification module with the features from the final convolutional layer of 4th stage (C4), and, alternatively, using *feature pyramid networks* (FPN) [24].

We assign videos from two different locations for the test phase and the others for training. All videos were sampled every 30 frames. During training, the positive samples are the RoIs with IoU scores greater than 0.5 with the ground truth, and all other RoIs are considered negative. All frames are resized so that the shortest edge does not exceed 800 pixels resolution while maintaining the aspect ratio. We used a *batch* of 4 images, sampling 32 RoIs (limited by the GPU memory) with a 1:1 ratio between positive and negative samples. The models are initialized with the weights of the ImageNET database and trained for 10k iterations with an initial learning rate of $\alpha = 0.002$, which is reduced to 10% of its value from iteration 6k, and again from the 8k iteration.

The Table II show the model results considering only the model outputs, without any post-processing. The model with

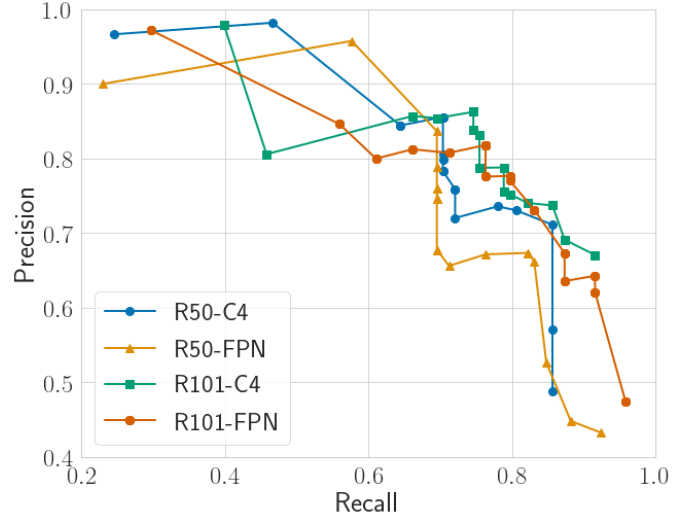


Figure 6: *Precision* \times *recall* obtained after post-processing within $v = 0.05 : 0.05 : 0.95$.

R50-C4 backbone had the lowest results in terms of AP_{50} e F_1 . The models with FPN (R50-FPN e R101-FPN) showed the highest scores in terms of AP_{50} . These models have the highest values of TP (91 and 89, respectively). However, they are also the ones with the highest values of FP (43 and 45, respectively). This implies in high recall values (Rc - 0.77 and 0.75, respectively) and low precision values (Pr - 0.68 and 0.66, respectively).

The model with R101-C4 presents TP values (87) close to those of the models that have the highest values (91 and 89); on the other hand, it is the one with the lowest value of FP (25), resulting in a good compromise between Pr and Rc, and, consequently, the highest value of F_1 .

B. Objects tracking

We applied the post-processing step, described in Section IV-B, with threshold $t_v = 0.4$, for the outputs of each model, to aggregate the temporal and spatial information present in the videos. It can be seen in the Table II that, except for the case of R50-FPN, this step improved the results in terms of both AP_{50} and F_1 . We increased the TP values of all models (again, except for the case of R50-FPN), sacrificing few FP (R101-C4) or even decreasing it (R50-C4 and R101-FPN). This resulted in a significant increase in Rc and a slight increase in Pr, reflecting an increase in F_1 .

The Figure 6 presents the *precision* \times *recall* curve for the results obtained by applying post-processing ranging from t_v from 5% to 95% with 5% step. As can be seen, as the value of t_v increases, there is a decrease in Rc and an increase in Pr. According to the necessity, the value of t_v can be adjusted to retrieve more objects, keeping in mind that more FPs are generated. The R50-C4 model reaches Pr close to 1.0 but with low Rc. The R50-FPN and R101-FPN models have high Rc but low Pr. This means higher amounts of FP. As previously noted, the model R101-C4 have the best trade-off between precision and recall, when compared to the other models.

Table II: Detection results before and after post-processing for different metrics.

Backbone	Post-processing	AP ₅₀	TP	FP	FN	Pr	Rc	F ₁
R50-C4	-	65.10	81	33	37	0.71	0.69	0.70
	$t_v = 0.4$	69.39	85	27	33	0.76	0.72	0.74
R50-FPN	-	72.85	91	43	27	0.68	0.77	0.72
	$t_v = 0.4$	68.45	84	44	34	0.66	0.71	0.68
R101-C4	-	71.19	87	25	31	0.78	0.74	0.76
	$t_v = 0.4$	74.94	93	30	25	0.76	0.79	0.77
R101-FPN	-	71.58	89	45	29	0.66	0.75	0.71
	$t_v = 0.4$	74.62	94	28	24	0.77	0.80	0.78

VI. CONCLUSION

In this work, we present a wide database of aerial images containing several objects commonly associated with potential mosquito breeding grounds. We also propose a system to detect objects of interest, acting in two stages. In the first step, detection is done frame by frame using the *Faster R-CNN* architecture, and a subsequent tracking step that registers successive detections. This additional processing can increase the true positives, significantly improving the performance of the system as a whole. The results obtained are promising. Using ResNet-101-FPN as *backbone*, it is possible to obtain an accuracy of 0.78 in terms of *F1-score*.

ACKNOWLEDGMENT

This study was financed in part by the Coordenação de Aperfeiçoamento de Pessoal de Nível Superior – Brasil (CAPES) – Finance Code 001; Fundação Carlos Chagas Filho de Amparo à Pesquisa do Estado do Rio de Janeiro (FAPERJ); Conselho Nacional de Desenvolvimento Científico e Tecnológico (CNPq); and Google Latin America Research Awards (LARA), 2019.

REFERENCES

- [1] C. Rückert, J. Weger-Lucarelli, S. M. Garcia-Luna *et al.*, “Impact of simultaneous exposure to arboviruses on infection and transmission by aedes aegypti mosquitoes,” *Nature Communications*, vol. 8, pp. 1–9, may 2017.
- [2] A. Laserna, J. Barahona-Correa, L. Baquero *et al.*, “Economic impact of dengue fever in latin america and the caribbean: A systematic review,” *Revista Panamericana de Salud Pública*, vol. 42, p. e111, sep 2018.
- [3] Pan American Health Organization, “Dengue in the Americas reaches highest number of cases recorded,” <https://reliefweb.int/report/world/dengue-americas-reaches-highest-number-cases-recorded>, 2019, accessed: 2020-03-22.
- [4] World Health Organization, “Zika virus,” <https://www.who.int/news-room/fact-sheets/detail/zika-virus>, 2018, accessed: 2020-03-22.
- [5] —, “Chikungunya,” <https://www.who.int/news-room/fact-sheets/detail/chikungunya>, 2017, accessed: 2020-03-22.
- [6] —, “Yellow fever – Brazil,” <https://www.who.int/csr/don/11-february-2019-yellow-fever-brazil/en/>, 2019, accessed: 2020-03-23.
- [7] L. Lambrechts and A. Failloux, “Vector biology prospects in dengue research,” *Memórias do Instituto Oswaldo Cruz*, vol. 107, no. 8, pp. 1080–1082, dec 2012.
- [8] H. Mao, X. Yang, and W. J. Dally, “A delay metric for video object detection: What average precision fails to tell,” *CoRR*, vol. abs/1908.06368, 2019. [Online]. Available: <http://arxiv.org/abs/1908.06368>
- [9] K. Bernardin, A. Elbs, and R. Stiefelhagen, “Multiple object tracking performance metrics and evaluation in a smart room environment,” *Proceedings of IEEE International Workshop on Visual Surveillance*, 01 2006.
- [10] A. Milan, K. Schindler, and S. Roth, “Challenges of ground truth evaluation of multi-target tracking,” in *2013 IEEE Conference on Computer Vision and Pattern Recognition Workshops*, 2013, pp. 735–742.
- [11] F. Yin, D. Makris, and S. Velastin, “Performance evaluation of object tracking algorithms,” *10th IEEE International Workshop on Performance Evaluation of Tracking and Surveillance (PETS2007)*, 01 2007.
- [12] A. Agarwal, U. Chaudhuri, S. Chaudhuri *et al.*, “Detection of Potential Mosquito Breeding Sites Based on Community Sourced Geotagged Images,” in *Geospatial InfoFusion and Video Analytics IV; and Motion Imagery for ISR and Situational Awareness II*, no. 3, jul 2014, p. 90890M.
- [13] M. G. Prasad, A. Chakraborty, R. Chalasani *et al.*, “Quadcopter-based Stagnant Water Identification,” in *IEEE National Conference on Computer Vision, Pattern Recognition, Image Processing and Graphics*, Patna, India, dec 2015, pp. 1–4.
- [14] M. Mehra, A. Bagri, X. Jiang, and J. Ortiz, “Image Analysis for Identifying Mosquito Breeding Grounds,” in *IEEE International Conference on Sensing, Communication and Networking (Workshop)*, London, UK, jun 2016, pp. 1–6.
- [15] P. Haddawy, P. Wettayakorn, B. Nonthaleerak *et al.*, “Large scale detailed mapping of dengue vector breeding sites using street view images,” *PLOS Neglected Tropical Diseases*, vol. 13, no. 7, pp. 1–27, jul 2019.
- [16] W. L. Passos, T. M. Dias, H. M. A. Junior *et al.*, “Acerca da detecção automática de focos do mosquito aedes aegypti,” in *Brazilian Symposium on Telecommunications and Signal Processing*, Campina Grande, Brazil, sep 2018, pp. 392–396.
- [17] T. M. Dias, V. C. Alves, H. M. Alves *et al.*, “Autonomous detection of mosquito-breeding habitats using an unmanned aerial vehicle,” in *2018 Latin American Robotic Symposium, 2018 Brazilian Symposium on Robotics (SBR) and 2018 Workshop on Robotics in Education (WRE)*, 2018, pp. 351–356.
- [18] B. D. Barros, “On data augmentation techniques for the automatic detection of mosquito breeding grounds using videos,” *Dissertação de mestrado*, Universidade Federal do Rio de Janeiro - COPPE/PEE, Rio de Janeiro, RJ, Brasil, 2019.
- [19] W. L. Passos, “Automatic aedes aegypti breeding grounds detection using computer vision techniques,” *Dissertação de mestrado*, Universidade Federal do Rio de Janeiro - COPPE/PEE, Rio de Janeiro, RJ, Brasil, 2019.
- [20] Z. Zhang, “A Flexible New Technique for Camera Calibration,” *IEEE Transactions on Pattern Analysis and Machine Intelligence (PAMI)*, vol. 22, no. 11, pp. 1330–1334, nov 2000.
- [21] Z. Zhao, P. Zheng, S. Xu, and X. Wu, “Object Detection With Deep Learning: A Review,” *IEEE Transactions on Neural Networks and Learning Systems*, vol. 30, no. 11, pp. 3212–3232, jan 2019.
- [22] S. Ren, K. He, R. Girshick, and J. Sun, “Faster R-CNN: Towards Real-Time Object Detection with Region Proposal Networks,” *IEEE Transactions on Pattern Analysis and Machine Intelligence (PAMI)*, vol. 39, no. 6, pp. 1137–1149, jun 2017.
- [23] B. S. Reddy and B. N. Chatterji, “An fft-based technique for translation, rotation, and scale-invariant image registration,” *IEEE Transactions on Image Processing*, vol. 5, no. 8, pp. 1266–1271, 1996.
- [24] T.-Y. Lin, P. Dollar, R. Girshick, K. He, B. Hariharan, and S. Belongie, “Feature Pyramid Networks for Object Detection,” in *IEEE Conference on Computer Vision and Pattern Recognition (CVPR)*, Honolulu, USA, jul 2017, pp. 936–944.